# Model reduction methods for population dynamics with fast-switching environments: Reduced master equations, stochastic differential equations, and applications

Peter G. Hufton,[1] Yen Ting Lin,[1,2] and Tobias Galla[1]

[1]*Theoretical Physics, School of Physics and Astronomy, University of Manchester, Manchester M13 9PL, United Kingdom*

[2]*Center for Nonlinear Studies and Theoretical and Biophysics Group, Theoretical Division, Los Alamos National Laboratory, Los Alamos, New Mexico 87545, USA*

(Received 14 January 2019; published 15 March 2019)

We study stochastic population dynamics coupled to fast external environments and combine expansions in the inverse switching rate of the environment and a Kramers–Moyal expansion in the inverse size of the population. This leads to a series of approximation schemes, capturing both intrinsic and environmental noise. These methods provide a means of efficient simulation and we show how they can be used to obtain analytical results for the fluctuations of population dynamics in switching environments. We place the approximations in relation to existing work on piecewise-deterministic and piecewise-diffusive Markov processes. Finally, we demonstrate the accuracy and efficiency of these model-reduction methods in different research fields, including systems in biology and a model of crack propagation.

DOI: 10.1103/PhysRevE.99.032122

## I. INTRODUCTION

The study of stochastic population dynamics, coupled to time-varying external environments, is a current challenge from point of view of both fast simulation techniques and the development of analytical tools. Stochastic populations are routinely simulated using the Gillespie algorithm. Analytical approximation techniques such as Kramers-Moyal or system-size expansions are available, but in their standard form they have mostly been developed for closed systems [1–3]. Applications in which varying external conditions are important include the modeling of bacterial populations subject to antibiotic treatment [4–7] or protein production in gene regulatory networks [8–12]. In this latter example it is the stochastic binding and unbinding of promoters that acts as the environmental process. Further applications are in evolutionary dynamics [13–16], disease spreading [17], and ecology and population dynamics [18–21]. Many of these examples combine the extrinsic environmental noise with intrinsic stochasticity, due to reactions in finite populations. Examples of systems coupled to stochastic external environments go as far as reliability analysis and crack propagation in materials, where environmental states correspond to different strains due to external loading [22–27].

Existing literature on random processes in external environments includes approaches based on stochastic differential equations (SDEs) coupled to continuous environments [13,28–30]. Alternatively, deterministic dynamics with discrete external noise has been considered, for example, in [31–33]. The quasi-steady-state approximation is used to eliminate fast reactions [34,35] in reaction systems in chemistry.

In the preceding paper [36] we developed reduction techniques for stochastic systems with discrete states coupled to fast external environments. More precisely, we showed how the environment can be integrated out to result in a reduced dynamics for the open classical system. The purpose of [36] is to establish the formalism to do this and to discuss the interpretation and limitations of the reduced dynamics. Importantly, no approximation of the intrinsic dynamics of the open system was made in [36]; the reduction methods developed there solely focused on approximating the environmental process.

In the present work we build on the preceding paper, to also approximate the dynamics of the population itself. The main result of this paper is a detailed description of how expansions in the inverse timescale of the environmental dynamics can be combined with expansions in the inverse system size of the population.

These are effectively weak-noise expansions for the extrinsic and intrinsic stochasticity of the problem, which in many cases facilitate analytical results or more efficient simulation. Using this approach, we obtain a number of different approximation schemes, each capturing the intrinsic and extrinsic noise to different degrees of accuracy. We put these different schemes in relation to each other and we also put them into context with existing approaches such as piecewise deterministic Markov processes [37–45] or piecewise diffusive dynamics [46–48]. We apply the formalism to a number of examples ranging from gene regulatory networks to crack propagation in materials.

The remainder of the paper is organized as follows. In Sec. II we introduce the general model setting, a classical stochastic system, coupled to an external environment, which moves stochastically between discrete sates. We summarize some of the results of [36], where we derived the reduced master equation in the limit of fast but not infinitely fast environmental dynamics. In Sec. III we then combine expansions in the inverse size of the population with that in the timescale of the switching dynamics and provide a systematic classification of the different model reduction schemes which result from this combined expansion. We discuss a set of applications in Sec. IV, before we summarize and present

 

our conclusions in Sec. V. The Appendixes contain further examples and details of some of our calculations.

## II. MODEL DEFINITIONS AND BACKGROUND

### A. Model

The general model setting is the same as in [36]. We study a stochastic system with discrete states $\ell$. In this paper this will generally be a population of individuals who can each be of different species, so that $\ell = (n_1, \ldots, n_S)$, where $n_i$ describes the number of individuals of each species in the population ($i = 1, \ldots, S$). We will often use the words "system" and "population" synonymously.

The dynamics of the system consists of reactions which either remove or create particles or convert one type of particle into another. One can think of these as birth and death events. The population is coupled to an environment. The environment also takes discrete states, labeled $\sigma$. The combined dynamics of the system and environment runs in continuous time and the dynamics of the system depends on the current state of the environment. The environment in turn switches between its states with transition rates which can depend on the state $\ell$ of the system.

The dynamics of the system and environment is described by the master equation

$$\frac{d}{dt}p(\ell,\sigma,t) = \mathcal{M}_\sigma p(\ell,\sigma,t) + \lambda\sum_{\sigma'} A_{\sigma'\to\sigma}(\ell)p(\ell,\sigma',t), \quad (1)$$

where $p(\ell,\sigma,t)$ is the joint probability of finding the system in state $\ell$ and the environment in state $\sigma$ at time $t$. The object $\mathcal{M}_\sigma$ is an operator and describes the changes of the state of the system when the environment is in state $\sigma$.

The term proportional to $\lambda$ in Eq. (1) represents the environmental switching. The rate with which the environment transitions from state $\sigma$ to state $\sigma'$ is $\lambda A_{\sigma\to\sigma'}(\ell)$. These can depend on the state $\ell$ of the system. The prefactor $\lambda > 0$ sets the timescale of the environment relative to the internal dynamics of the population. Large values of $\lambda \gg 1$ indicate a fast environmental process. We use the convention $A_{\sigma\to\sigma}(\ell) = -\sum_{\sigma'\neq\sigma} A_{\sigma\to\sigma'}(\ell)$ for the diagonal elements of the matrix $\mathbf{A}(\ell)$.

### B. Reduced master equation

We first focus on the case in which the dynamics of the environment is independent of the state of the population, i.e., we assume that the $A_{\sigma\to\sigma'}$ do not depend on $\ell$. We are interested in the case when the environment is fast, $\lambda \gg 1$, and write $\rho^*(\sigma|\ell)$ for the stationary distribution of the environmental process, given a fixed state $\ell$ of the population. Making the ansatz

$$p(\ell,\sigma,t) = \rho^*(\sigma|\ell)\Pi(\ell,t) + \frac{1}{\lambda}w_\sigma(\ell,t) \quad (2)$$

and adapting a calculation in [31], we showed in [36] that the marginal distribution $\Pi(\ell,t) = \sum_\sigma p(\ell,\sigma,t)$ fulfills the equation

$$\frac{d}{dt}\Pi(\ell,t) = \sum_\sigma \mathcal{M}_\sigma[\rho^*(\sigma|\ell)\Pi(\ell,t)] + \frac{1}{\lambda}\sum_\sigma \mathcal{M}_\sigma w_\sigma(\ell,t). \quad (3)$$

This approximation captures terms to subleading order in $\lambda^{-1}$. The leading-order contribution to $w_\sigma(\ell,t)$ can be found from the relation [36]

$$\sum_{\sigma'} A_{\sigma'\to\sigma}(\ell)w_{\sigma'}(\ell,t) = \rho^*(\sigma|\ell)\sum_{\sigma'}\mathcal{M}_{\sigma'}[\rho^*(\sigma'|\ell)\Pi(\ell,t)] - \mathcal{M}_\sigma[\rho^*(\sigma|\ell)\Pi(\ell,t)]. \quad (4)$$

Together Eqs. (3) and (4) describe the time evolution of $\Pi(\ell,t)$, neglecting corrections of order $\lambda^{-2}$ and higher. We note that the physical interpretation in terms of a random process has limitations; this is discussed in detail in [36]. We will nevertheless call Eq. (3) the reduced master equation.

Focusing on the case in which there are two environmental states and the environmental process is independent of the state of the population, we further showed in [36] that the reduced master equation simplifies to

$$\frac{d}{dt}\Pi(\ell,t) = \mathcal{M}_{\rm avg}\Pi(\ell,t) + \frac{1}{2}\frac{\theta^2}{\lambda}(\mathcal{M}_0 - \mathcal{M}_1)^2\Pi(\ell,t), \quad (5)$$

where

$$\theta^2 = \frac{2k_0k_1}{(k_0+k_1)^3} \quad (6)$$

and $\mathcal{M}_{\rm avg} = \sum_\sigma \rho^*_\sigma M_\sigma$. The stationary distribution of the environmental process $\rho^*$ does not depend on $\ell$ when the environment switches independently of the population.

We will refer to the case in which the timescale separation between the population dynamics and environmental process is infinite ($\lambda \to \infty$) as the adiabatic limit. In this situation one has

$$\frac{d}{dt}\Pi(\ell,t) = \mathcal{M}_{\rm avg}\Pi(\ell,t) \quad (7)$$

for the example with a population-independent environment. In the more general case one finds, from Eq. (3),

$$\frac{d}{dt}\Pi(\ell,t) = \sum_\sigma \mathcal{M}_\sigma[\rho^*(\sigma|\ell)\Pi(\ell,t)]. \quad (8)$$

We note a separate approach to approximating environmental noise in the fast-switching limit which involves assuming a large number of environmental states so that the environment may be approximated as continuous [49,50].

### C. Objective of the present work

Established methods for the approximation of Markovian processes in population dynamics involves carrying out an asymptotic expansion in powers of the inverse size of the population. In the absence of the complication of environmental switching, this typically is achieved by performing either the Kramers-Moyal expansion or van Kampen's system-size expansion [1,2]. These techniques are commonly used in a number of applications of population dynamics; they have recently been extended to the case of jump processes in switching environments [46–48]. Following such an expansion, the state

of the population is continuous and, for a fixed environmental state, described by a stochastic or ordinary differential equation. Alternative approaches, based on the Wentzel-Kramers-Brillouin (WKB) method, have been pursued, for example, in Refs. [11,13,19,29,30,51]. These approaches, however, do not provide a dynamical description of the population, but focus on stationary or quasistationary states.

The purpose of this paper is to combine Kramers-Moyal-type expansions with the expansion in the timescale separation between the environment and population described in Sec. II B. This leads to different levels of *dynamical* description depending on how the environmental switching and the discreteness and intrinsic stochasticity of the population are treated. Studying these different levels of approximation is also useful to put our results into the context of existing work [12,31–33,35,37–48,52–58]. We will first give a general overview and then consider a specific example.

## III. EXPANSION IN SYSTEM SIZE

### A. Overview

A schematic overview is given in Fig. 1. We use the notation $\Omega$ to describe the typical size of the population. Broadly speaking the overall picture involves expansions in the inverse switching timescale $\lambda^{-1}$ and/or the inverse population size $\Omega^{-1}$. The parameters $\lambda$ and $\Omega$ correspond to the vertical and horizontal directions, respectively, in Fig. 1. In the top row we perform no expansion in $\lambda^{-1}$ (i.e., we keep all terms), in the middle row we assume $\lambda \gg 1$ but finite (keeping leading and subleading terms), and in the bottom row the adiabatic limit has been taken ($\lambda \to \infty$), i.e., the noise due to the environmental switching is discarded altogether. The left-hand column describes models with a discrete population (arbitrary $\Omega$), in the middle column we assume $\Omega \gg 1$ but finite, and in the right-hand column the limit $\Omega \to \infty$ has been taken, i.e., all intrinsic noise in the population is disregarded. We now discuss the relation between the different levels of approximation in more detail.

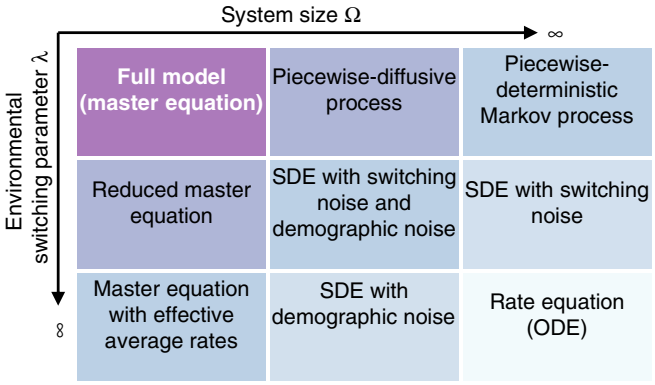


FIG. 1. Schematic overview of the different model-reduction schemes for populations coupled to external environments with discrete states. Each column and row corresponds to a successive layer of approximation.

#### 1. Expansion in environmental timescale

In Sec. II B we focused on the left-hand column of Fig. 1. The top left box is the full microscopic model, involving a discrete population of typical size $\Omega$ and an environmental process associated with a switching timescale set by $\lambda$. This full model is defined by the master equation (1). Expanding to subleading order in $\lambda^{-1}$ but keeping $\Omega$ fixed and general, one obtains the reduced master equation (3), as indicated in the middle box in the left-hand column in Fig. 1. The limit $\lambda \to \infty$ is the adiabatic limit, and one finds the master equation (7). This is the bottom left-hand box in Fig. 1. As discussed in more detail in [36], Eq. (7) describes a process with the same types of reactions as the original dynamics, but with rates that are weighted averages over the stationary distribution of the environmental states. This is conceptually similar to the quasi-steady-state approximation [34,35,53–55,58], in which the fast-reacting species are regarded as constant at values obtained from an appropriate weighted average. We stress again that there are limitations to the physical interpretation of this equation, in particular during short-term transients. This is discussed in [36].

#### 2. Expansion in powers of inverse system size

In a different approach one can first approximate the intrinsic noise for large system size ($\Omega \gg 1$), starting from the full model (environment and population), without any expansion in the environmental switching timescale. This is done by carrying out a Kramers-Moyal expansion on the dynamics of the population while simultaneously maintaining the discrete environmental states [48]. This corresponds to moving horizontally along the top row of Fig. 1.

If subleading-order terms in powers of the inverse system size are retained, one obtains piecewise-diffusive dynamics [46–48,59], corresponding to the middle box in the first row of Fig. 1. In this approximation the population is described by a stochastic differential equation between switches of the environmental state. The combined process of the environment and population is approximated by

$$\frac{\partial}{\partial t} p_\sigma(\mathbf{x}, t) = \mathcal{F}_\sigma p_\sigma(\mathbf{x}, t) + \lambda \sum_{\sigma'} A_{\sigma' \to \sigma} p_\sigma(\mathbf{x}, t), \qquad (9)$$

where $p_\sigma(\mathbf{x}, t)$ is a probability density over continuous states $\mathbf{x}$, obtained from discrete states $\ell$ in the limit of large $\Omega$ (see Sec. III B 1 for a specific example). The $\mathcal{F}_\sigma$ are Fokker-Planck operators obtained from a Kramers-Moyal expansion on $\mathcal{M}_\sigma$.

#### 3. Combined expansion

Starting from the piecewise-diffusive process [top row, middle box in Fig. 1, Eq. (9)] one can follow the same steps as in Sec. II B and consider the limit of fast but not infinitely fast environmental switching. In Fig. 1 this means moving down the middle column. In considering the simultaneous limits of large $\Omega$ and large $\lambda$, we assume that the ratio $\Omega/\lambda$ remains finite. This will become more clear in the example discussed below (Sec. III B 1). For the case of two environmental states, one starts from Eq. (9), in which the limit $\Omega \gg 1$ has been taken, but where $\lambda$ is still general. The only difference between Eqs. (9) and (1) is the replacement of $\mathcal{M}_\sigma$ by $\mathcal{F}_\sigma$.

The result of an expansion in powers of $\lambda^{-1}$ can then be read off from Eq. (5) by simply replacing $\mathcal{M}_\sigma$ by $\mathcal{F}_\sigma$, i.e.,

$$\frac{\partial}{\partial t}\Pi(\mathbf{x},t) = \mathcal{F}_{\rm avg}\Pi(\mathbf{x},t) + \frac{1}{2}\frac{\theta^2}{\lambda}(\mathcal{F}_0 - \mathcal{F}_1)^2\Pi(\mathbf{x},t). \quad (10)$$

An interpretation of Eq. (10) in terms of a stochastic differential equation can be obtained by expanding the term $(\mathcal{F}_0 - \mathcal{F}_1)^2$ further and keeping only terms to order $1/\Omega$. This stochastic differential equation contains two different sources of Gaussian noise, one representing demographic noise and the other the stochasticity of the environmental switching. This is the center box in Fig. 1. We will illustrate this using specific examples below.

Finally, we could also take the adiabatic limit $\lambda \to \infty$; this leads to $\frac{\partial}{\partial t}\Pi(\mathbf{x},t) = \mathcal{F}_{\rm avg}\Pi(\mathbf{x},t)$. In this limit, the noise due to the environmental process has been eliminated entirely and the resulting SDE contains only Gaussian noise coming from the intrinsic fluctuations in the population. This is indicated in the bottom box of the middle column in Fig. 1.

#### 4. Piecewise-deterministic process

We can also take the limit of an infinite population $\Omega \to \infty$ first, keeping $\lambda$ general. Thus, we neglect intrinsic fluctuations altogether. This is achieved by retaining only the leading-order term in the Kramers-Moyal expansion of the population. In each fixed environment the dynamics of the population is then described by an ordinary differential equation (ODE). This constitutes what is known as a piecewise-deterministic Markov process (PDMP) [37,38]. In Fig. 1 this is the right-hand box in the top row. Mathematically, the PDMP is described by

$$\frac{\partial}{\partial t}p_\sigma(\mathbf{x},t) = \mathcal{L}_\sigma p_\sigma(\mathbf{x},t) + \lambda\sum_{\sigma'}A_{\sigma'\to\sigma}p_\sigma(\mathbf{x},t), \quad (11)$$

with Liouville operators $\mathcal{L}_\sigma$; they are first-order differential operators which describe the deterministic drift of the system in a given environmental state.

We can now use the PDMP as a starting point and move down the right-hand column of Fig. 1, following the same steps as before (Sec. II B), replacing $\mathcal{M}_\sigma$ by $\mathcal{L}_\sigma$. For two environmental states and keeping terms of order $\lambda^{-1}$, the result is analogous to Eqs. (5) and (10). One finds

$$\frac{\partial}{\partial t}\Pi(\mathbf{x},t) = \mathcal{L}_{\rm avg}\Pi(\mathbf{x},t) + \frac{1}{2}\frac{\theta^2}{\lambda}(\mathcal{L}_0 - \mathcal{L}_1)^2\Pi(\mathbf{x},t). \quad (12)$$

This is a Fokker-Planck equation and corresponds to an SDE in which Gaussian noise reflects the effects of the fast-switching environment, indicated in the middle box of the right-hand column in Fig. 1. Equations of this type were previously reported in Ref. [31].

A further approximation to the dynamics would again involve taking the adiabatic limit: This is equivalent to ignoring the final term in Eq. (12). The resulting Liouville equation corresponds to an ODE description of the system. Its dynamics is then governed by a rate equation, where the reaction rates are weighted averages over the different environmental states. In such an approximation all stochasticity, both intrinsic and environmental, has been eliminated. This is the bottom entry in the right-hand column of Fig. 1.

### B. Simple examples

#### 1. Population with one species

We now focus on an example of a population with a single type of particles and an environment with two states. The purpose of this basic example is purely illustrative; specific applications will be discussed in Sec. IV. Particles are produced at constant rate $\beta\Omega$ and they are removed with per capita rates $\delta_\sigma$ in environments $\sigma \in \{0, 1\}$. We have

$$\mathcal{M}_\sigma = \beta\Omega(\mathcal{E}^{-1} - 1) + \delta_\sigma(\mathcal{E} - 1)n, \quad (13)$$

where $n$ is the number of particles in the population. The operator $\mathcal{E}$ acts on functions of $n$ and is defined as $\mathcal{E}f(n) = f(n+1)$.

Keeping the system-size parameter $\Omega$ fixed and taking the limit of large but finite $\lambda$, one obtains

$$\begin{aligned}\frac{d}{dt}\Pi(n) &= \Omega\beta(\mathcal{E}^{-1} - 1)\Pi(n)\\ &\quad + (\mathcal{E} - 1)\left[\delta_{\rm avg} - \frac{\theta^2}{\lambda}(\delta_0 - \delta_1)^2(2n-1)\right]n\Pi(n)\\ &\quad + \frac{1}{2}\frac{\theta^2}{\lambda}(\delta_0 - \delta_1)^2[\mathcal{E}^2 - 1]n(n-1)\Pi(n). \quad (14)\end{aligned}$$

This corresponds to the middle box in the left-hand column of Fig. 1, and we note that the last term in this reduced dynamics describes reactions in which two particles are removed simultaneously. Such reactions are not present in the original dynamics; see [36] for a detailed discussion of the interpretation and the limits of reduced master equations of this type.

Taking $\lambda \to \infty$ in Eq. (14), one has

$$\frac{d}{dt}\Pi(n,t) = \Omega\beta(\mathcal{E}^{-1} - 1)\Pi(n,t) + (\mathcal{E} - 1)\delta_{\rm avg}n\Pi(n,t), \quad (15)$$

where $\delta_{\rm avg} = (k_1\delta_0 + k_0\delta_1)/(k_0 + k_1)$; this is the master equation with effective average rates (bottom box on the left in Fig. 1).

Next, writing $x = n/\Omega$ and starting again from the full model of population and environment, we carry out a Kramers-Moyal expansion first (keeping terms up to subleading order in $1/\Omega$). One finds the Fokker-Planck operators

$$\begin{aligned}\mathcal{F}_0 &= \beta\left(-\partial_x + \frac{1}{2\Omega}\partial_x^2\right) + \delta_0\left(\partial_x + \frac{1}{2\Omega}\partial_x^2\right)x,\\ \mathcal{F}_1 &= \beta\left(-\partial_x + \frac{1}{2\Omega}\partial_x^2\right) + \delta_1\left(\partial_x + \frac{1}{2\Omega}\partial_x^2\right)x.\end{aligned} \quad (16)$$

These operators, together with Eq. (9), describe a piecewise-diffusive process (top row, middle column in Fig. 1); in a given environmental state the dynamics is described by an Itô SDE

$$\dot{x} = \beta - \delta_{\sigma(t)}x + \sqrt{\frac{\beta + \delta_{\sigma(t)}x}{\Omega}}\eta(t), \quad (17)$$

where $\eta(t)$ is Gaussian white noise of unit variance.

Further approximating the piecewise-diffusive process in the limit of fast environmental switching, we can insert the explicit form of $\mathcal{F}_\sigma$ into Eq. (10) to give

$$\begin{aligned}\frac{\partial}{\partial t}\Pi(x,t) &= -\partial_x\left\{\left[\beta - \delta_{\rm avg}x + \tfrac{1}{2}g_e\partial_x g_e\right]\Pi(x,t)\right\}\\ &\quad + \tfrac{1}{2}\partial_x^2\left\{\left[g_i^2 + g_e^2\right]\Pi(x,t)\right\}, \quad (18)\end{aligned}$$

where $\Delta = \delta_0 - \delta_1$ and

$$g_i(x)^2 = \frac{1}{\Omega}(\beta + \delta_{\rm avg} x), \tag{19}$$

$$g_e(x)^2 = \frac{\theta^2}{\lambda}\Delta^2 x^2. \tag{20}$$

The subscript $i$ indicates intrinsic stochasticity (demographic noise) and $e$ labels the contribution to the noise from environmental switching. We note that $g_i(x)^2 \propto \Omega^{-1}$ and $g(x)_e^2 \propto \lambda^{-1}$. It is interesting to note that the same Fokker-Planck equation is obtained by a direct Kramers-Moyal expansion of Eq. (14). Details can be found in Appendix A 1. The contribution $g_e \partial_x g_e/2$ to the drift term in Eq. (18) is of order $\lambda^{-1}$ and it can safely be neglected to the order we are working at (see also Ref. [31]). Equation (18) then describes an Itô SDE of the form

$$\dot{x} = \beta - \delta_{\rm avg} x + g_i(x)\eta_i(t) + g_e(x)\eta_e(t), \tag{21}$$

in which $\eta_i(t)$ and $\eta_e(t)$ are independent Gaussian processes of unit variance and with no correlations in time. The SDE (21) corresponds to the center box in Fig. 1.

Equation (18) can be used as a starting point for further approximations. In the case of infinitely fast switching $\lambda \to \infty$ the term $g_e(x)$ can be neglected and one finds

$$\frac{\partial}{\partial t}\Pi(x,t) = -\partial_x[(\beta - \delta_{\rm avg} x)\Pi(x,t)] + \frac{1}{2\Omega}\partial_x^2[(\beta + \delta_{\rm avg} x)\Pi(x,t)]. \tag{22}$$

We note that this relation can also be obtained by direct Kramers-Moyal expansion of Eq. (15). Only the Gaussian noise from the intrinsic stochasticity then remains in the SDE (21). This is the bottom box in the middle column of Fig. 1.

In the case of an infinite population $\Omega \to \infty$, Eq. (18) turns into

$$\frac{\partial}{\partial t}\Pi(x,t) = -\partial_x[(\beta - \delta_{\rm avg} x)\Pi(x,t)] + \frac{\theta^2}{2\lambda}\Delta^2\partial_x^2[x^2\Pi(x,t)], \tag{23}$$

so the noise term containing $g_i(x)$ is no longer present in the SDE (21). This is the middle box in the right-hand column of Fig. 1. Equation (23) can also be found from Eq. (12) upon using $\mathcal{L}_\sigma \Pi(x) = -\partial_x(\beta - \delta_\sigma x)\Pi(x)$ (see Appendix A 2).

If all stochasticity is ignored altogether ($\lambda \to \infty$ and $\Omega \to \infty$) one has $g_i = g_e = 0$. In our example one then finds the rate equation

$$\dot{x} = \beta - \delta_{\rm avg} x. \tag{24}$$

This corresponds to the bottom box in the right-hand column of Fig. 1.

#### *2. Population dynamics with two species*

We next consider an example already used in [36]. In this system there are two types of particles, labeled $A$ and $B$; they are removed with constant per capita rates $\gamma$ and $\delta$, respectively. Particles are created with rates $\Omega\alpha_\sigma$ and $\Omega\beta_\sigma$. These production rates depend on the state of the environment, as indicated by the subscript, and as before we assume two environmental states $\sigma \in \{0, 1\}$, with switching dynamics as before. The state of the population can be written as $\ell = (n_A, n_B)$, where $n_A$ is the number of particles of type $A$ and $n_B$ the number of particles of type $B$. One then has

$$\mathcal{M}_\sigma = \Omega\alpha_\sigma\left(\mathcal{E}_A^{-1} - 1\right) + \gamma(\mathcal{E}_A - 1)n_A + \Omega\beta_\sigma\left(\mathcal{E}_B^{-1} - 1\right) + \delta(\mathcal{E}_B - 1)n_B, \tag{25}$$

where $\mathcal{E}_A f(n_A, n_B) = f(n_A + 1, n_B)$ and similarly for $\mathcal{E}_B$.

The reduced master equation for this model is derived in [36]. Carrying out a Kramers-Moyal expansion in powers of $\Omega^{-1}$ and retaining leading and subleading terms, we arrive at the stochastic differential equations for $x_A = n_A/\Omega$ and $x_B = n_B/\Omega$,

$$\begin{aligned} \dot{x}_A &= \alpha_{\rm avg} - \gamma x_A + \eta_A(t), \\ \dot{x}_B &= \beta_{\rm avg} - \delta x_B + \eta_B(t). \end{aligned} \tag{26}$$

For compactness, we have absorbed the diffusion coefficients (describing both intrinsic and extrinsic noise) into the white noise terms $\eta_A$ and $\eta_B$, so they have the covariance matrix

$$\begin{aligned} \langle \eta_A(t)\eta_A(t')\rangle &= \left(\frac{\alpha_{\rm avg} + \gamma x_A}{\Omega} + \frac{\theta^2}{\lambda}(\Delta\alpha)^2\right)\delta(t - t'), \\ \langle \eta_B(t)\eta_B(t')\rangle &= \left(\frac{\beta_{\rm avg} + \delta x_B}{\Omega} + \frac{\theta^2}{\lambda}(\Delta\beta)^2\right)\delta(t - t'), \\ \langle \eta_A(t)\eta_B(t')\rangle &= \frac{\theta^2}{\lambda}\Delta\alpha\Delta\beta\delta(t - t') \end{aligned} \tag{27}$$

(see also Appendix B). We have introduced $\Delta\alpha = \alpha_0 - \alpha_1$ and $\Delta\beta = \beta_0 - \beta_1$. This again corresponds to the center box in Fig. 1 and we note that the noise contains contributions from the intrinsic stochasticity (terms proportional to $\Omega^{-1}$ in the variance) and from the environmental noise (terms proportional to $\lambda^{-1}$).

To simplify matters we now restrict the discussion to the case $\gamma = \delta$ and $\alpha_{\rm avg} = \beta_{\rm avg}$ (the latter does not imply $\Delta\alpha = \Delta\beta$). In the long run the deterministic trajectory, obtained from Eq. (26) in the combined limit $\lambda \to \infty$ and $\Omega \to \infty$, converges to the fixed point given by $x_A^* = x_B^* = \alpha_{\rm avg}/\gamma$. Writing $x_A(t) = x^* + \zeta_A(t)$ and $x_B(t) = x_B^* + \zeta_B(t)$ and applying the linear-noise approximation (LNA) [1,2] at the fixed point, we find

$$\begin{aligned} \dot{\zeta}_A &= -\gamma\zeta_A + \eta_A(t), \\ \dot{\zeta}_B &= -\gamma\zeta_B + \eta_B(t), \end{aligned} \tag{28}$$

where

$$\begin{aligned} \langle \eta_A(t)\eta_A(t')\rangle &= \left(\frac{2\alpha_{\rm avg}}{\Omega} + \frac{\theta^2}{\lambda}(\Delta\alpha)^2\right)\delta(t - t'), \\ \langle \eta_B(t)\eta_B(t')\rangle &= \left(\frac{2\alpha_{\rm avg}}{\Omega} + \frac{\theta^2}{\lambda}(\Delta\beta)^2\right)\delta(t - t'), \\ \langle \eta_A(t)\eta_A(t')\rangle &= \frac{\theta^2}{\lambda}\Delta\alpha\Delta\beta\delta(t - t'). \end{aligned} \tag{29}$$

In order to test these results we proceed and find analytical predictions for the spectral density of fluctuations about the fixed point. To do this we perform a Fourier transform and

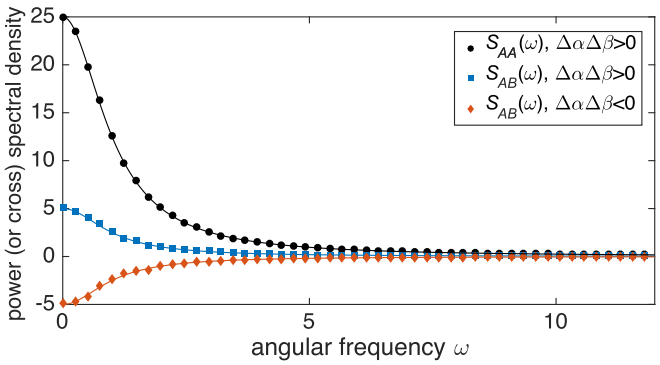


FIG. 2. Spectra of fluctuations from direct simulations of the full model (closed symbols) and from the linear-noise approximation of the effective SDE capturing intrinsic and extrinsic noise ($k_0 = k_1 = 1$, $\Omega = 20$, $\lambda = 20$, $\alpha_0 = 0$, $\alpha_1 = 1$, and $\Delta t = 0.1$).

obtain

$$\begin{aligned}\langle\hat{\zeta}_A(\omega)\hat{\zeta}_A^*(\omega')\rangle &= \delta(\omega+\omega')\Omega^{-2}S_{AA}(\omega),\\ \langle\hat{\zeta}_A(\omega)\hat{\zeta}_B^*(\omega')\rangle &= \delta(\omega+\omega')\Omega^{-2}S_{AB}(\omega),\end{aligned} \tag{30}$$

with

$$\begin{aligned}S_{AA}(\omega) &= \Omega^2\frac{\frac{2\alpha_{\rm avg}}{\Omega}+\frac{\theta^2}{\lambda}(\Delta\alpha)^2}{\gamma^2+\omega^2},\\ S_{AB}(\omega) &= \Omega^2\frac{\frac{\theta^2}{\lambda}\Delta\alpha\Delta\beta}{\gamma^2+\omega^2}.\end{aligned} \tag{31}$$

As can be seen in Fig. 2, this result matches well with the results of Gillespie simulating the full model (for $\Omega = 20$ and $\lambda = 20$). We had previously used the power spectral density of fluctuations to test simulation procedures for populations in fast-switching environments [36]. Adding to this, the derivation of the SDE (26) and (27) and the subsequent LNA provides a tool to calculate these spectra analytically.

## IV. APPLICATIONS

In this section we will use the formalism we have developed to a series of specific examples. Further applications are discussed in Appendix D.

### A. Bimodal genetic switch

#### 1. Model

We now discuss a stylized model of a genetic circuit in pluripotent stem cells. These have the ability to differentiate into several possible cell types [44,60,61]; the basic features of the networks of genes, transcription factors, and epigenetic variables leading to these cell-fate decisions are a current focus of research [62–65]. Several hypotheses exist about the mechanisms leading to cell differentiation; among these it has been proposed that excursions of the genetic circuit into different areas of state space might contribute to steering cells towards distinct differentiated states [60,61]. Bimodal distributions are observed in a variety of biological switches [29,39,66–68].

In this section we discuss a stylized model of processes leading to bimodal distributions; the difference from the model in the preceding section is that this extended model admits a multimodal stationary distribution. In the context of the above hypothesis, these different peaks would lead to distinct differentiated states.

The model describes a single gene $G$, with a promoter site which can bind to a total of up to $N$ molecules of protein. Each protein molecule binds with a rate $\lambda k_+/\Omega$ and unbinds with a rate $k_-$. Binding and unbinding are sequential [69]. Depending on the current state of the gene (i.e., the number of bound proteins $\sigma = 0, 1, \ldots, N$), mRNA molecules are produced with rate $\Omega b_\sigma$. In turn, mRNA decays with (per capita) rate $d$; its presence also leads to the production of protein molecules, which occurs with a rate $\beta$ per mRNA molecule. Protein molecules finally decay with rate $\delta$. The model can be summarized by the reactions

$$\begin{aligned}G_\sigma + P &\underset{\lambda k_-}{\overset{\lambda k_+/\Omega}{\rightleftharpoons}} G_{\sigma+1} \quad \text{for } \sigma < N,\\ G_\sigma &\xrightarrow{\Omega b_\sigma} G_\sigma + M,\\ M &\xrightarrow{d} \emptyset, \quad M \xrightarrow{\beta} M + P, \quad P \xrightarrow{\delta} \emptyset,\end{aligned} \tag{32}$$

where $M$ and $P$ refer to molecules of mRNA and protein, respectively.

Mathematically, the two main differences compared to the models in the previous sections are the following: (i) The environment (the gene) can take more than two states ($\sigma = 0, 1, \ldots, N$) and (ii) the overall rate with which switches from state $\sigma$ to $\sigma + 1$ occur ($\sigma < N$) depends on the number of protein. Each protein molecule contributes $\lambda k_+/\Omega$ to the switching rate; the total rate of switching from state $\sigma < N$ to $\sigma + 1$ is $\lambda k_+ N_p/\Omega$ if the number of proteins is $N_p$. This means that the environmental switching depends on the state of the population.

Different architectures of the genetic switching and associated mRNA-production rates are discussed in the literature, e.g., [45,62,64,65,70]. We focus on $N = 2$, i.e., there are three possible environmental states $\sigma = 0, 1, 2$. We also assume that mRNA molecules are produced with a common basal rate in gene states $\sigma = 0, 1$, i.e., we set $b_0 = b_1$. When a maximum of $N = 2$ proteins are bound to the gene mRNA is produced with the activated rate $\Omega b_2$, where $b_2 > b_0$ [44].

#### 2. Comparison of the different approximation schemes

We test the eight different approximations in Fig. 1. In order to derive the reduced master equation, we need to go beyond Eq. (5), as there are more than two environmental states and because the environmental switching depends on the state of the population of mRNA and proteins. The construction therefore starts from Eqs. (3) and (4), with three environmental states $\sigma \in \{0, 1, 2\}$. The calculation leading to the reduced master equation for this model is tedious, but straightforward. The expression for the reduced master equation is lengthy and given in Appendix C 1.

For large but finite $\Omega$, the piecewise-diffusive process for this model is described by

$$\begin{aligned}\dot{m} &= (b_{\sigma(t)} - dm) + \Omega^{-1/2}\sqrt{b_{\sigma(t)} + dm}\,\eta^m(t),\\ \dot{p} &= (\beta m - \delta p) + \Omega^{-1/2}\sqrt{\beta m + \delta p}\,\eta^p(t).\end{aligned} \tag{33}$$

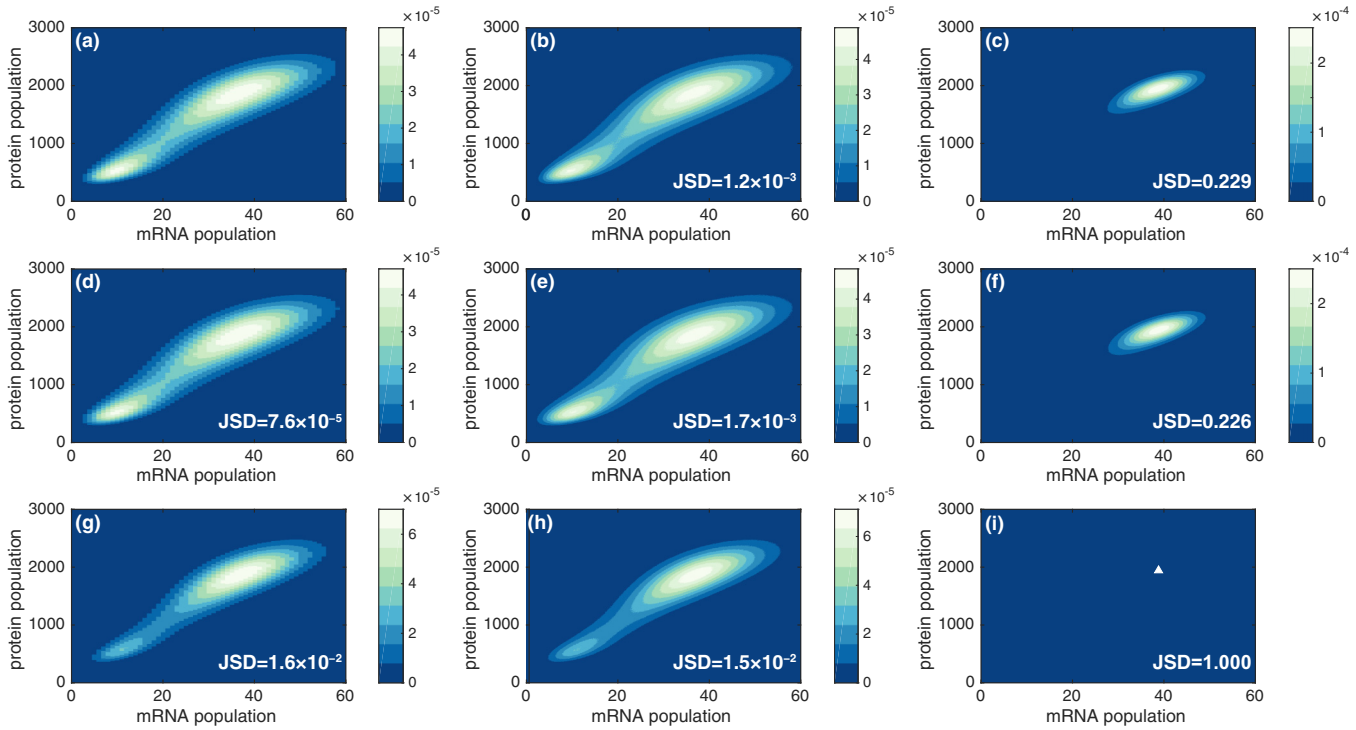


FIG. 3. Stationary probability distribution of the populations of mRNA and protein molecules for the full model in Sec. IV A and the eight levels of model reduction in Fig. 1: (a) full model, (b) piecewise-diffusive process, (c) piecewise-deterministic Markov process, (d) reduced master equation, (e) SDE with switching noise and demographic noise, (f) SDE with switching noise, (g) master equation with average rates, (h) SDE with demographic noise, and (i) rate equation (▲ represents a $\delta$ peak). The parameters are $N = 2$, $\Omega = 50$, $b_0 = b_1 = 1$, $b_2 = 20$, $d = 9.2$, $\beta = 50$, $\delta = 1$, $k_- = 0.025$, $k_+ = 1$, and $\lambda = 1250$.

For fast environmental switching, the approximation corresponding to the central box in Fig. 1 is given by the stochastic differential equations

$$\begin{aligned} \dot{m} &= [b_{\text{avg}}(p) - dm] + \left[g_i^m(m,p)^2 + g_e^m(m,p)^2\right]^{1/2}\eta^m(t), \\ \dot{p} &= (\beta m - \delta p) + g_i^p(m,p)\eta^p(t), \end{aligned} \tag{34}$$

where we have

$$\begin{aligned} b_{\text{avg}}(p) &= \frac{b_0 k_-^2 + b_0 k_- k_+ p + b_2 k_+^2 p^2}{k_-^2 + k_- k_+ p + k_+^2 p^2}, \\ g_e^m(m,p) &= \sqrt{\frac{2k_- k_+^2 p^2 [k_-^2 + 3k_- k_+ p + k_+^2 p^2]}{\lambda(k_-^2 + k_- k_+ p + k_+^2 p^2)^3}(b_2 - b_0)^2}, \\ g_i^m(m,p) &= \Omega^{-1/2}\sqrt{b_{\text{avg}}(p) + dm}, \\ g_i^p(m,p) &= \Omega^{-1/2}\sqrt{\beta m + \delta p}. \end{aligned} \tag{35}$$

From this it is straightforward to obtain further approximations by sending the amplitude of either the intrinsic noise ($g_i^m$ and $g_i^p$) or the environmental noise ($g_e^m$) to zero or both.

Figure 3 shows the stationary distributions obtained for the full model and for the different approximations. All data are from direct simulations, except Fig. 3(d), which is discussed further below. The arrangement corresponds to that in the schematic of Fig. 1, and for each approximation we report the Jensen-Shannon divergence (JSD) relative to the stationary distribution of the full model in Fig. 3(a). The JSD in Fig. 3(f) is lower than that in Fig. 3(d). This is due to the following effect. The full model in Fig. 3(a) can explore arbitrary numbers of mRNA and protein molecules. The stationary distribution of the PDMP in Fig. 3(c) however has bounded support, because intrinsic noise is discarded. The distribution in Fig. 3(f) does not include effects of intrinsic noise either, but the environmental stochasticity has been approximated by Gaussian noise, restoring an unbounded support. This leads to the seemingly better agreement of Fig. 3(f) with the full model. A similar effect is seen upon comparing Figs. 3(h) and 3(g).

The figure also demonstrates that the bimodal structure of the stationary distribution is induced by the intrinsic noise; it is present in each panel in the left-hand and middle columns, but in none of the panels in the right-hand column. We note in particular that the model only has one single fixed point in the deterministic limit, in contrast to other models of genetic switches which have been studied with the WKB method [29]. While the model is stylized and not intended to directly model a particular biological system, Fig. 3 demonstrates that analyses of this type may help to establish the origin of relevant biological features; in this case bimodality linked to pluripotency and cell-fate decision making is due to intrinsic rather than extrinsic noise.

On a technical note, we add that the approximation in Fig. 3(d), the reduced master equation, does not in itself define a Markovian process for this model, due to the appearance of negative rates (see Appendix C 1); further details of reduced master equations with negative rates are discussed in [36]. We have generated the data for the stationary distribution of the

reduced master equation in two different ways. One is direct numerical integration of the reduced master equation, which leads to a JSD relative to the distribution for the full model of approximately $7.6 \times 10^{-5}$. The second method consists of Gillespie simulations of an approximation to the reduced master equation [see Eq. (C1)], in which subleading terms of order $\Omega^2/\lambda$ are kept, but those of order $\Omega/\lambda$ are discarded; specifically, we have set $\varpi_1 = \varpi_2 = 0$ in Eq. (C1) for the purpose of these simulations. This leads to a Markovian process, and sample paths can hence be generated using the standard Gillespie algorithm. The JSD for the stationary distribution obtained in this way from that of the full model is found to be approximately $9.1 \times 10^{-5}$. Visually, the results from the two methods are indistinguishable and their JSD from each other is approximately $1.3 \times 10^{-5}$, almost an order of magnitude lower than the JSD of either of the two from the stationary distribution of the full model.

#### 3. *Efficient simulations and required computing time*

Although we have carried out all eight different approximations in the previous example, we remark that some are more useful than others in terms of providing an efficient simulation scheme for specific applications. The purpose of collating data from the different levels of model reduction in Fig. 3 was to give an illustration of the schematic in Fig. 1 in the context of a concrete example.

The approximation as an SDE (center panel in Figs. 1 and 3) provides a good starting point for simulations of systems with intrinsic noise of small and moderate amplitude and fast-switching environments. The SDE is an approximation, but it retains both intrinsic and extrinsic noise. In the context of simpler models, we have already used the SDE to carry out further mathematical analysis using the LNA (see Sec. III B 2). To further illustrate the possible advantages of the approximation as an SDE, we have investigated the amount of computing time needed to carry out simulations of the full model in Eq. (32) and of the SDE (34). Broadly speaking, the number of environmental switching events per unit time in the full model can be expected to scale as $\lambda$ and the number of events in the population per unit time grows as $\Omega$. One would therefore expect the computing time required to generate a given number of sample paths for the full model up to a specified end time to grow when $\lambda$ or $\Omega$ is increased. This is confirmed in Table I. The time required to generate sample paths of the SDE (34), however, is independent of $\lambda$ and $\Omega$, as these only enter in the noise strength. These results indicate that simulations of the SDE can be carried out more efficiently than those of the full model, especially when either the environmental switching is fast or the typical population size is large, or both. This is also the regime in which the SDE approximation becomes increasingly accurate.

TABLE I. Comparison of the simulation time of the full model (32) and the SDE (34). The Gillespie algorithm and Euler-Maruyama method ($dt = 5 \times 10^{-3}$) are used, respectively, to simulate the system up to time $10^4$. While the simulation time of the full model increases with $\lambda$ and $\Omega$, the simulation time for the SDE is independent of $\lambda$ and $\Omega$.

| $\lambda$ | $\Omega$ | Computation time (s) for the full model | Computation time (s) for the SDE with switching and demographic noise |
|---|---|---|---|
| 500 | 50 | 62.4 | 34.3 |
| 1000 | 50 | 74.0 | 34.4 |
| 1500 | 50 | 85.0 | 34.4 |
| 2000 | 50 | 93.2 | 34.4 |
| 1250 | 20 | 40.4 | 34.5 |
| 1250 | 40 | 67.4 | 34.7 |
| 1250 | 60 | 95.7 | 34.4 |
| 1250 | 80 | 123.2 | 34.3 |

### B. Genetic circuit with exclusive binding

Next we consider a circuit with exclusive promoter binding [71,72]. The model describes two genes $G^A$ and $G^B$ and two corresponding proteins $P^A$ and $P^B$. Proteins $P^A$ and $P^B$ bind to genes of the opposing type $G^B$ and $G^A$, respectively, with (per capita) rates $\lambda\kappa_1/\Omega$ and $\lambda\mu_1/\Omega$. They unbind from these promoters with rates $\lambda\kappa_0$ and $\lambda\mu_0$. These binding and unbinding reactions can be summarized as

$$G^A_{\text{unbnd}} + G^B_{\text{unbnd}} \underset{\lambda\kappa_0}{\overset{n_B\lambda\kappa_1/\Omega}{\rightleftharpoons}} G^A_{\text{bnd}} + G^B_{\text{unbnd}},$$
$$G^A_{\text{unbnd}} + G^B_{\text{unbnd}} \underset{\lambda\mu_0}{\overset{n_A\lambda\mu_1/\Omega}{\rightleftharpoons}} G^A_{\text{unbnd}} + G^B_{\text{bnd}}, \tag{36}$$

where the subscripts bnd and unbnd indicate whether the gene is bound to a protein or unbound, respectively, and where $n_A$ and $n_B$ are the numbers of molecules of proteins of types $A$ and $B$. In this model either gene $G^A$ or gene $G^B$ can be bound, but not both simultaneously. This is due to spatial considerations of the binding process: Owing to the protein size and the proximity of the genes, the binding of a particular protein blocks the other protein from binding [71,72]. When gene $G^A$ is bound, proteins of type $A$ are produced with rate $\Omega\alpha_0$, and when it is unbound, they are produced with rate $\Omega\alpha_1$. Similarly, when gene $G^B$ is bound, proteins of type $B$ are produced with rate $\Omega\beta_0$, and when it is unbound, they are produced with rate $\Omega\beta_1$. To summarize, the protein production rates in the three gene configurations are as follows:

| Gene configuration | Production rate $P^A$ | Production rate $P^B$ |
|---|---|---|
| $G^A$, $G^B$ unbound | $\Omega\alpha_1$ | $\Omega\beta_1$ |
| $G^A$ bound | $\Omega\alpha_0$ | $\Omega\beta_1$ |
| $G^B$ bound | $\Omega\alpha_1$ | $\Omega\beta_0$ |

In this model one protein inhibits the expression of the other, i.e., $\alpha_0 < \alpha_1$ and $\beta_0 < \beta_1$. Additionally, protein $A$ degrades with rate $\gamma$ and protein $B$ with rate $\delta$.

In this model the birth rates of the two types of proteins are not independent; rather, they are connected through the state of the environment (the binding status of the two genes). Furthermore, when production of one protein is inhibited (for example, protein $A$ when $G^A$ is bound), the other protein is expressed with a higher rate ($G^B$ unbound). This is an example of a model of the kind considered in [36], where we show how anticorrelations lead to negative rates in the reduced master equation. The reduced master equation for this model is lengthy; we present it in Appendix C 2.

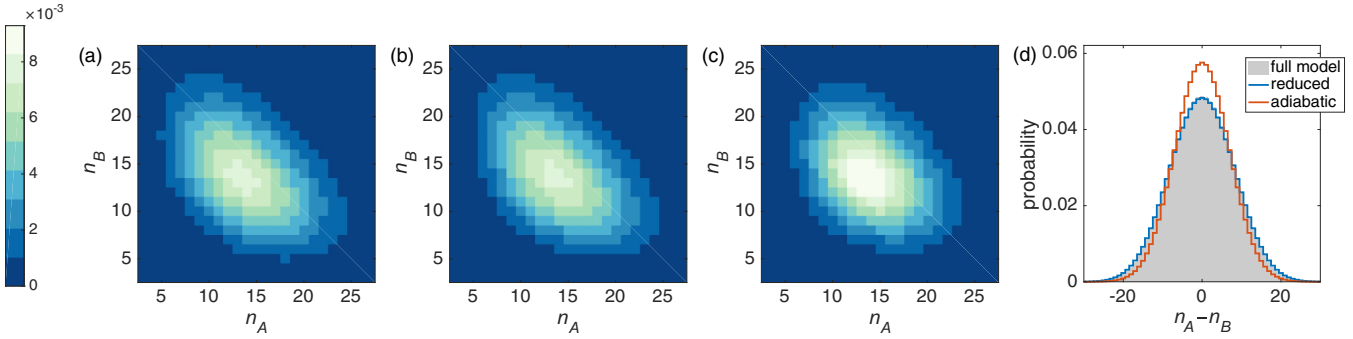


FIG. 4. Stationary distribution for the genetic circuit with exclusive binding (Sec. IV B) from numerical integration of (a) the full master equation with explicit environment, (b) the reduced master equation (C4), and (c) the adiabatic approximation which considers average rates. Also shown is (d) the marginal distribution of $n_A - n_B$ in order to compare the three distributions. The parameters are $\alpha_0 = \beta_0 = 0$, $\alpha_1 = \beta_1 = 1$, $\Omega = 20$, $\lambda\kappa_0 = \lambda\kappa_1 = 20$, and $\gamma = \delta = 1$.

Figure 4 shows the results for the stationary distribution obtained from numerical integration of this reduced master equation; we also show the stationary distributions of the full model and of the adiabatic approximation. As can be seen in Fig. 4(d), the reduced master equation reproduces the stationary distribution of the full model with greater accuracy than the adiabatic approximation.

### C. Reliability analysis and crack propagation

The formalism we have developed can also be applied to the calculation of time to failure in models of industrial systems. One of the challenges in this field is to capture features of real-world systems in tractable mathematical models. In this context, many authors have used piecewise-deterministic processes with Markovian external environments. These models incorporate discrete environmental effects such as different modes of operation, external stresses, or loads [25–27]. In these applications there is often a clear separation of timescales; the environmental switching is a much faster process than the degradation of the system. For example, a piece of material may be subject to mechanical load which changes several times a day or hour and the degradation of the material occurs over months or years.

Specifically, we consider the example of fatigue crack growth; this is an engineering problem describing the growth in the length of a crack in a mechanical component. One such model uses a piecewise-deterministic Markov process to describe the growth of the length of a crack [22–24,73] as

$$\dot{x} = x^b \times v_{\sigma(t)}, \tag{37}$$

where $x$ is the crack length, the exponent $b > 0$ is a constant, and as before $\sigma(t)$ represents the state of the environment at time $t$. The factor $v_\sigma$ takes into account that the crack grows faster in some environments than in others. Transitions from state $\sigma$ to $\sigma'$ occur with rate $\lambda A_{\sigma\to\sigma'}$.

Given an initial length $x_0$, we are interested in the time it takes to reach the threshold length $x = L$; this is when the component is deemed unreliable. We use the formalism of the earlier sections to approximate the PDMP as an SDE in the limit of fast (but not infinitely fast) environmental switching ($\lambda \gg 1$). We then find the first-passage time of this SDE through the threshold value. While diffusive processes have been used as starting points in models of reliability [74,75], we systematically reduce the PDMP to an effective stochastic differential equation.

In the simplest case of two environmental states (and writing $A_{0\to1} = k_1$ and $A_{1\to0} = k_0$ as before), Eq. (37) can be approximated by the SDE,

$$\dot{x} = x^b v_{\text{avg}} + g x^b \eta(t), \tag{38}$$

where

$$v_{\text{avg}} = \frac{k_0 v_0 + k_1 v_1}{k_0 + k_1}, \quad g^2 = \frac{2k_0 k_1 (v_0 - v_1)^2}{\lambda (k_0 + k_1)^3}. \tag{39}$$

Higher-order terms in $\lambda^{-1}$ have been discarded. For the special case of exponential growth $b = 1$, the SDE approximation turns into geometric Brownian motion. In a different context this has been implemented in Ref. [31]. We proceed to find the first-passage time of the process in Eq. (38) through the threshold $L$. This can be done following Ref. [76], but with a modification allowing for $b \neq 1$. As a first step we apply the transformation

$$y = \begin{cases} \ln x, & b = 1 \\ \frac{x^{1-b}-1}{1-b}, & b \neq 1. \end{cases} \tag{40}$$

The SDE (38) can then be written

$$\dot{y} = v_{\text{avg}} + g\eta(t). \tag{41}$$

For such a process, the distribution of first-passage times through a given threshold is known [76]. Returning to the original variables, we obtain the probability density $Q(x_0, t)$ of first-passage times of the process (38) through $L$, if started at position $x_0$ at time $t = 0$. For $b = 1$ one finds

$$Q(x_0, t) = \frac{|\ln(L/x_0)|}{gt(2\pi t)^{1/2}} \exp\left( -\frac{\left[\ln(L/x_0) - \left(v_{\text{avg}} - \frac{g^2}{2}\right)t\right]^2}{2g^2 t} \right), \tag{42}$$

and for $b \neq 1$ one has

$$Q(x_0, t) = \frac{1}{gt(2\pi t)^{1/2}} \left| \frac{L^{1-b} - x_0^{1-b}}{1-b} \right| \times \frac{-\left[\left(L^{1-b} - x_0^{1-b}\right)/(1-b) - \left(v_{\text{avg}} - \frac{g^2}{2}\right)t\right]^2}{2g^2 t}. \tag{43}$$

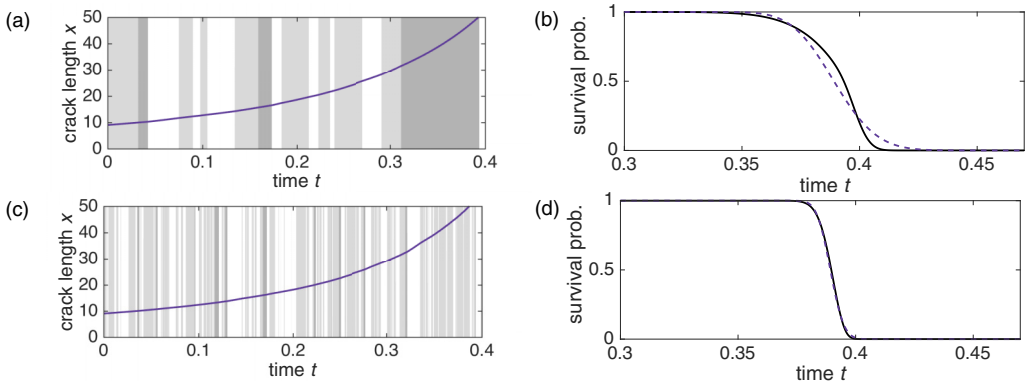


FIG. 5. (a) Sample path of the model of crack growth (Sec. IV C). Background shading indicates the state of the environment, with states 0, 1, and 2 shown progressively darker. (b) Survival probability as a function of time. The black line shows results from Monte Carlo simulations and the dashed line is the prediction of Eq. (43). (c) and (d) Same quantities as in (a) and (b), respectively, for tenfold increased switching rates. The model parameters are given in the text.

This approach can be extended to models with more than two environmental states, leading to modifications in the noise strength $g$. We demonstrate this with a numerical example. We use the parameters suggested in Ref. [73], in particular $b = 1.5$ and

$$\lambda \mathbf{A} = \begin{bmatrix} -40 & 40 & 0 \\ 54 & -60 & 6 \\ 20 & 0 & -20 \end{bmatrix}, \quad v = \begin{bmatrix} 1.0 \\ 0.9 \\ 1.2 \end{bmatrix}.$$

The initial crack length is $x_0 = 9$, and we use $L = 50$ as the threshold for the onset of failure. Compared to Ref. [73], we have rescaled time. Implementing our theory shows that the process can be approximated by the SDE (38) where $v_{\mathrm{avg}} = 69/70$ and $g^2 = 141/274\,400$. This is obtained from solving Eq. (4) with a numerical algebra package, again replacing the operator $\mathcal{M}_\sigma$ with the appropriate Liouville operator. Figure 5(a) shows a sample path of the PDMP generated by Monte Carlo simulation, while the background indicates the state of the environment. Figure 5(b) shows the probability that a given component is still reliable at time $t$. The black line is obtained through Monte Carlo simulations, whereas the dashed line is the prediction of Eq. (43). For the specified parameters, the two lines show agreement. Increasing the switching rate [Fig. 5(d)] strengthens this agreement.

## V. SUMMARY AND CONCLUSIONS

We have developed methods for the reduction and approximation of the dynamics of populations' coupled external environments with a finite number of discrete states. Our analysis focuses on the limit in which the environmental dynamics is fast relative to that of the system, but where the timescale separation is not necessarily infinite. We have combined expansions in the timescale separation with expansions in the inverse size of the population.

As a key result, we derive a stochastic differential equation for the population, capturing both intrinsic and environmental noise. This stochastic differential equation provides a starting point for efficient numerical studies. Simulating the dynamics of the original population and the discrete environment is costly, especially if the population is large or when the dynamics of the environment is very fast. The amount of computing time needed to integrate the SDE however is independent of the population size and the speed of the environmental dynamics. At the same time, the approximation leading to the SDE becomes increasingly more accurate when the population is large and the environmental dynamics fast. We have also demonstrated that the SDE can be used to obtain further analytical results; for example, spectral properties of fluctuations can be computed analytically within the linear-noise approximation.

We placed our reduction schemes in the context of existing work on piecewise-deterministic Markov processes and piecewise-diffusive processes. This provides a more complete picture of different approximations for systems with intrinsic noise and environmental fluctuations. It may hence help to select the most appropriate approximation method for specific applications.

We have demonstrated how these results can be used to study a number of problems in different areas. We discussed models of genetic circuits and of crack propagation. Further applications in the Appendixes include cases in which the switching between external conditions is non-Markovian and a more complex genetic network with multiple genes. These applications are only a selected set of examples of situations in which switching environments play a role. We expect that the model-reduction schemes will be of use for the analytical and numerical investigation of further classical open systems in biology and the physical sciences, as well as in other disciplines.

## ACKNOWLEDGMENTS

P.G.H., Y.T.L., and T.G. thank the Engineering and Physical Sciences Research Council for funding (Ph.D. studentship and Grant No. EP/K037145/1). Y.T.L. was supported by the Center for Nonlinear Studies.

All authors contributed equally to this work.

## APPENDIX A: FURTHER DETAILS OF THE ANALYSIS OF THE MODEL IN SEC. III B 1

### 1. Kramers-Moyal expansion of the reduced master equation

In this Appendix we carry out a direct Kramers-Moyal expansion of the reduced master equation (14). This master equation can be written as

$$\frac{d}{dt}\Pi(n,t) = \Omega\beta(\mathcal{E}^{-1}-1)\Pi(n) + (\mathcal{E}-1)\delta_{\rm eff} n\Pi(n,t) + \frac{1}{2}\frac{\theta^2}{\lambda}\Delta^2[\mathcal{E}^2-1]n(n-1)\Pi(n,t), \tag{A1}$$

where $\Delta = \delta_0 - \delta_1$ and

$$\delta_{\rm eff} = \delta_{\rm avg} - \frac{1}{2}\frac{\theta^2}{\lambda}\Delta^2(2n-1). \tag{A2}$$

To carry out the expansion we write $\mathcal{E}^2 = 1 + \frac{2}{\Omega}\partial_x + \frac{2}{\Omega^2}\partial_x^2 + \cdots$ and obtain (writing $x = n/\Omega$)

$$\frac{\partial}{\partial t}\Pi(x) = \beta\left(-\partial_x + \frac{1}{2\Omega}\partial_x^2\right)\Pi(x) + \left(\partial_x + \frac{1}{2\Omega}\partial_x^2\right)\delta_{\rm eff} x\Pi(x) + \frac{1}{2}\frac{\theta^2}{\lambda}\Omega\Delta^2\left(2\partial_x + \frac{2}{\Omega}\partial_x^2\right)x\left(x-\frac{1}{\Omega}\right)\Pi(x), \tag{A3}$$

where neglected terms are of order $1/\Omega^2$ or of order $\frac{\theta^2}{\lambda}/\Omega \propto 1/\lambda\Omega$. There will be further terms in Eq. (A3) which can be neglected at the order we are working at. Next we collect terms

$$\frac{\partial}{\partial t}\Pi(x) = -\partial_x\left\{\left[\beta - \delta_{\rm eff}x - \frac{\theta^2}{\lambda}\Omega\Delta^2 x\left(x-\frac{1}{\Omega}\right)\right]\Pi(x)\right\} + \frac{1}{2\Omega}\partial_x^2\left\{\left[\beta + \delta_{\rm eff}x + 2\frac{\theta^2}{\lambda}\Omega\Delta^2x^2\right]\Pi(x)\right\}, \tag{A4}$$

where another term of order $1/\lambda\Omega$ has been dropped. Now we use $\delta_{\rm eff} = \delta_{\rm avg} - \frac{1}{2}\frac{\theta^2}{\lambda}\Omega\Delta^2(2x - \frac{1}{\Omega})$ and find

$$\begin{aligned}\frac{\partial}{\partial t}\Pi(x) = &-\partial_x\left\{\left[\beta - \delta_{\rm avg}x + \frac{1}{2}\frac{\theta^2}{\lambda}\Omega\Delta^2 x\left(2x-\frac{1}{\Omega}\right) - \frac{\theta^2}{\lambda}\Omega\Delta^2 x\left(x-\frac{1}{\Omega}\right)\right]\Pi(x)\right\}\\ &+ \frac{1}{2\Omega}\partial_x^2\left\{\left[\beta + \delta_{\rm avg}x - \frac{\theta^2}{\lambda}\Omega\Delta^2x^2 + 2\frac{\theta^2}{\lambda}\Omega\Delta^2x^2\right]\Pi(x)\right\},\end{aligned} \tag{A5}$$

where yet another term of order $1/\lambda\Omega$ has been dropped. This is the same as

$$\frac{\partial}{\partial t}\Pi(x) = -\partial_x\left\{\left[\beta - \delta_{\rm avg}x + \frac{1}{2}\frac{\theta^2}{\lambda}\Delta^2 x\right]\Pi(x)\right\} + \frac{1}{2}\partial_x^2\left\{\left[\frac{1}{\Omega}(\beta + \delta_{\rm avg}x) + \frac{\theta^2}{\lambda}\Delta^2x^2\right]\Pi(x)\right\}, \tag{A6}$$

i.e., we recover Eq. (18).

### 2. Reduced Liouville equation

Using $\mathcal{L}_\sigma\Pi(x) = -\partial_x(\beta - \delta_\sigma x)\Pi(x)$ in Eq. (12) gives

$$\frac{\partial}{\partial t}\Pi = -\partial_x(\beta - \delta_{\rm avg}x)\Pi(x) + \frac{1}{2}\frac{\theta^2}{\lambda}\Delta^2\partial_x x\partial_x x\Pi(x). \tag{A7}$$

Next we use $\partial_x[x\partial_x x\Pi(x)] = \partial_x^2(x^2\Pi) - \partial_x(x\Pi)$ to write this as

$$\frac{\partial}{\partial t}\Pi = -\partial_x\left(\beta - \delta_{\rm avg}x + \frac{1}{2}\frac{\theta^2}{\lambda}\Delta^2 x\right)\Pi(x) + \frac{1}{2}\frac{\theta^2}{\lambda}\Delta^2\partial_x^2[x^2\Pi(x)]. \tag{A8}$$

Neglecting the term $\frac{1}{2}g_e\partial_x g_e = \frac{1}{2}\frac{\theta^2}{\lambda}\Delta^2 x$, this is Eq. (23).

## APPENDIX B: KRAMERS-MOYAL EXPANSION FOR THE TWO-SPECIES MODEL IN SEC. III B 2

The reduced master equation for the two-species model is derived in [36] and reads

$$\begin{aligned}\frac{d}{dt}\Pi = &\gamma(\mathcal{E}_A - 1)n_A\Pi + \delta(\mathcal{E}_B - 1)n_B\Pi + \Omega\alpha_{\rm eff}\left(\mathcal{E}_A^{-1} - 1\right)\Pi + \Omega\beta_{\rm eff}\left(\mathcal{E}_B^{-1} - 1\right)\Pi\\ &+ \frac{\Omega^2\theta^2}{2\lambda}(\Delta\alpha)^2\left(\mathcal{E}_A^{-2} - 1\right)\Pi + \frac{\Omega^2\theta^2}{2\lambda}(\Delta\beta)^2\left(\mathcal{E}_B^{-2} - 1\right)\Pi + \frac{\Omega^2\theta^2}{\lambda}\Delta\alpha\Delta\beta\left(\mathcal{E}_A^{-1}\mathcal{E}_B^{-1} - 1\right)\Pi,\end{aligned} \tag{B1}$$

where $\Delta\alpha \equiv \alpha_0 - \alpha_1$, $\Delta\beta \equiv \beta_0 - \beta_1$, and

$$\begin{aligned}\alpha_{\rm eff} &= \alpha_{\rm avg} - \frac{\Omega\theta^2}{\lambda}(\Delta\alpha)^2 - \frac{\Omega\theta^2}{\lambda}\Delta\alpha\Delta\beta,\\ \beta_{\rm eff} &= \beta_{\rm avg} - \frac{\Omega\theta^2}{\lambda}(\Delta\beta)^2 - \frac{\Omega\theta^2}{\lambda}\Delta\alpha\Delta\beta.\end{aligned} \tag{B2}$$

Carrying out the Kramers-Moyal expansion on Eq. (B1) we find

$$\frac{\partial}{\partial t}\Pi(x) = \gamma\left(\partial_x + \frac{1}{2\Omega}\partial_x^2\right)x\Pi + \delta\left(\partial_y + \frac{1}{2\Omega}\partial_y^2\right)y\Pi + \alpha_{\rm eff}\left(-\partial_x + \frac{1}{2\Omega}\partial_x^2\right)\Pi + \beta_{\rm eff}\left(-\partial_y + \frac{1}{2\Omega}\partial_y^2\right)\Pi$$
$$+ \frac{\Omega\theta^2}{2\lambda}(\Delta\alpha)^2\left(-2\partial_x + \frac{2}{\Omega}\partial_x^2\right)\Pi(t) + \frac{\Omega\frac{\theta^2}{\lambda}}{2}(\Delta\beta)^2\left(-2\partial_y + \frac{2}{\Omega}\partial_y^2\right)\Pi$$
$$+ \frac{\Omega\theta^2}{\lambda}\Delta\alpha\Delta\beta\left(-\partial_x - \partial_y + \frac{1}{2\Omega}\partial_x^2 + \frac{1}{2\Omega}\partial_y^2 + \frac{1}{\Omega}\partial_x\partial_y\right)\Pi. \tag{B3}$$

Using Eq. (B2), this simplifies to

$$\frac{\partial}{\partial t}\Pi(x) = -\partial_x(\alpha_{\rm avg} - \gamma x)\Pi - \partial_y(\beta_{\rm avg} - \delta y)\Pi + \frac{1}{2}\partial_x^2\left(\frac{\alpha_{\rm avg} + \gamma x}{\Omega} + \frac{\theta^2}{\lambda}\Delta\alpha^2\right)\Pi$$
$$+ \frac{1}{2}\partial_y^2\left(\frac{\beta_{\rm avg} + \delta y}{\Omega} + \frac{\theta^2}{\lambda}\Delta\beta^2\right)\Pi + \partial_x\partial_y\left(\frac{\theta^2}{\lambda}\Delta\alpha\Delta\beta\right)\Pi, \tag{B4}$$

which describes the dynamics of the stochastic differential equations (26) and (27).

## APPENDIX C: APPLICATIONS: FURTHER DETAILS

### 1. Reduced master equation for the bistable genetic circuit

In this Appendix we report the reduced master equation for the model described in Sec. IV A. The reduced master equation is obtained starting from Eq. (3), where the $w_\sigma(\ell)$ are determined from (4). We do not report the full calculation; it is laborious, but ultimately straightforward. The final result for the reduced master equation reads

$$\frac{d}{dt}\Pi(N_p, N_m, t) = \left(E_m^{-1} - 1\right)\left\{\Omega\beta_{\rm avg}(N_p) - \frac{1}{\lambda}\Omega^2(\beta_2 - \beta_0)^2\frac{1}{k_-}\frac{2\psi^2}{(1+\psi+\psi^2)^3}[\psi^2 + 3\psi + 1]\right\}\Pi$$
$$+ (E_m - 1)[\delta_m N_m\Pi] + \left(E_p^{-1} - 1\right)[\alpha N_m + \varpi_1]\Pi + (E_p - 1)[\delta_p N_p + \varpi_2]\Pi$$
$$+ \left(E_m^{-2} - 1\right)\left[\frac{1}{\lambda}\Omega^2(\beta_2 - \beta_0)^2\frac{1}{k_-}\frac{\psi^2}{(1+\psi+\psi^2)^3}[\psi^2 + 3\psi + 1]\Pi\right]$$
$$+ \left(E_m^{-1}E_p^{-1} - 1\right)(-\varpi_1\Pi) + \left(E_m^{-1}E_p - 1\right)(-\varpi_2\Pi), \tag{C1}$$

where we have introduced the following shorthand ($\sigma = 0, 1, 2$):

$$\psi(N_p) = \frac{k_+ N_p}{\Omega k_-},$$
$$\rho_\sigma^*(N_p) = \frac{\psi(N_p)^{\sigma-1}}{1 + \psi(N_p) + \psi(N_p)^2},$$
$$\Delta_\sigma(N_p) = \rho_\sigma^*(N_p + 1) - \rho_\sigma^*(N_p),$$
$$\beta_{\rm avg}(N_p) = \sum_\sigma \rho_\sigma^*(N_p)\beta_\sigma,$$
$$\varpi_1 = \frac{1}{\lambda}\Omega(\beta_2 - \beta_0)\frac{1}{k_-}\{[\rho_0^*(N_p + 1) + \rho_1^*(N_p + 1)]\Delta_2 - \rho_1^*(N_p + 1)\Delta_0\}\alpha N_m,$$
$$\varpi_2 = \frac{1}{\lambda}\Omega(\beta_2 - \beta_0)\frac{1}{k_-}\{\rho_1^*(N_p - 1)\Delta_0(N_p - 1) - [\rho_0^*(N_p - 1) + \rho_1^*(N_p - 1)]\Delta_2(N_p - 1)\}\delta_p N_p. \tag{C2}$$

We note that $\varpi_1 > 0$, irrespective of the choice of $\lambda$, so the rate of the penultimate reaction in Eq. (C1) is negative. The rates of all other reactions are non-negative, provided $\lambda$ is large enough (all other parameters fixed).

### 2. Gene circuit with exclusive binding

In this Appendix we report the reduced master equation for the gene circuit with exclusive binding, discussed in Sec. IV B. Labeling the states $G^A$ and $G^B$ not occupied, only $G^A$ occupied, and only $G^B$ occupied as $\sigma = 0$, 1, and 2, respectively, we have the transition matrix elements

$$A_{0\to1} = n_A\mu_1/\Omega, \quad A_{0\to2} = n_B\kappa_1/\Omega, \quad A_{1\to0} = \kappa_0, \quad A_{2\to0} = \mu_0, \tag{C3}$$

where all other off-diagonal entries are zero and the diagonal elements follow from the convention $\sum_{\sigma'} A_{\sigma\to\sigma'} = 0$. For the purposes of the numerical analysis we make the simplifications $\alpha_0 = \beta_0$, $\alpha_1 = \beta_1$, $\kappa_0 = \mu_0$, and $\kappa_1 = \mu_1$, as well as $\gamma = \delta$. The reduced master equation in the limit of large but finite $\lambda$ is then obtained as

$$\begin{aligned}
\frac{d}{dt}P_{n_A,n_B}(t) &= \left(\mathcal{E}_A^{-1}-1\right)\left\{\Omega\frac{n_B\alpha_1\tilde\kappa_1+\alpha_0(\kappa_0+n_A\tilde\kappa_1)}{\kappa_0+(n_A+n_B)\tilde\kappa_1}-\frac{\Omega^2}{\lambda}\frac{2n_B\kappa_0\tilde\kappa_1(\alpha_0-\alpha_1)^2}{[\kappa_0+(n_A+n_B)\tilde\kappa_1]^3}\right\}P_{n_A,n_B}(t)\\
&+\left(\mathcal{E}_B^{-1}-1\right)\left\{\Omega\frac{n_A\alpha_1\tilde\kappa_1+\alpha_0(\kappa_0+n_B\tilde\kappa_1)}{\kappa_0+(n_A+n_B)\tilde\kappa_1}-\frac{\Omega^2}{\lambda}\frac{2n_A\kappa_0\tilde\kappa_1(\alpha_0-\alpha_1)^2}{[\kappa_0+(n_A+n_B)\tilde\kappa_1]^3}\right\}P_{n_A,n_B}(t)\\
&+\left(\mathcal{E}_A^{-2}-1\right)\frac{\Omega^2}{\lambda}\frac{n_B\tilde\kappa_1\left[\kappa_0^2+2n_A\kappa_0\tilde\kappa_1+n_A(n_A+n_B)\tilde\kappa_1^2\right](\alpha_0-\alpha_1)^2}{\kappa_0[\kappa_0+(n_A+n_B)\tilde\kappa_1]^3}P_{n_A,n_B}(t)\\
&-\left(\mathcal{E}_A^{-1}\mathcal{E}_B^{-1}-1\right)\frac{\Omega^2}{\lambda}\frac{2n_An_B\tilde\kappa_1^2[2\kappa_0+(n_A+n_B)\tilde\kappa_1](\alpha_0-\alpha_1)^2}{\kappa_0[\kappa_0+(n_A+n_B)\tilde\kappa_1]^3}P_{n_A,n_B}(t)\\
&+\left(\mathcal{E}_B^{-2}-1\right)\frac{\Omega^2}{\lambda}\frac{n_A\tilde\kappa_1[\kappa_0^2+2n_B\kappa_0\tilde\kappa_1+n_B(n_A+n_B)\tilde\kappa_1^2](\alpha_0-\alpha_1)^2}{\kappa_0[\kappa_0+(n_A+n_B)\tilde\kappa_1]^3}P_{n_A,n_B}(t)\\
&+\gamma\left(\mathcal{E}_A^{+1}-1\right)n_AP_{n_A,n_B}(t)+\gamma\left(\mathcal{E}_B^{+1}-1\right)n_BP_{n_A,n_B}(t),
\end{aligned}\tag{C4}$$

where $\tilde\kappa_1$ has been introduced as shorthand for $\kappa_1/\Omega$. We have discarded terms of order $\Omega/\lambda$.

## APPENDIX D: FURTHER APPLICATIONS

### 1. Genetic network with multiple genes

A related model, as considered in Ref. [12], involves $N$ identical promoter genes $G^{(i)}$ $(i = 1,\dots,N)$, which can each be in their on or off states and switch between these independently. This is different from the model in Appendix C, where a single gene can bind up to $N$ molecules of protein. The $N$ genes operate in parallel; for the dynamics of the population only the total number of genes in each state matters. As a consequence, there are $N+1$ different environmental states describing the configuration of the genes. We use the number of genes in the on state to label these states $\sigma \in \{0,\dots,N\}$. We leave out the mRNA dynamics and focus only on protein production and decay. We assume that each gene in its on state contributes $\Omega b_1$ to the total production rate and each gene in its off state contributes $\Omega b_0$. As before, the parameter $\Omega$ controls the typical size of the population of protein molecules. We then have $\Omega b_\sigma = (N-\sigma)\Omega b_0 + \sigma\Omega b_1$ for the total production rate. The model is defined by the reactions

$$\begin{aligned}
&G_{\rm off}^{(i)} \xrightarrow{\Omega b_0} G_{\rm off}^{(i)} + P, \quad G_{\rm off}^{(i)} \underset{\lambda k_0}{\overset{\lambda k_1}{\rightleftharpoons}} G_{\rm on}^{(i)},\\
&G_{\rm on}^{(i)} \xrightarrow{\Omega b_1} G_{\rm on}^{(i)} + P, \quad P \xrightarrow{\delta} \emptyset,
\end{aligned}\tag{D1}$$

where the reactions for different genes $i = 1,\dots,N$ run independently. The SDE description of the model in the limit of large but finite $\Omega$ and $\lambda$ is of the form

$$\dot p = Nb_{\rm avg} - \delta p + [g_i(p)^2 + g_e(p)^2]^{1/2}\eta(t), \tag{D2}$$

where each gene contributes an average rate of production $b_{\rm avg} = (b_0k_0 + b_1k_1)/(k_0+k_1)$. The contribution to the noise from intrinsic fluctuations has amplitude

$$g_i(p)^2 = \frac{1}{\Omega}(Nb_{\rm avg} + \delta p). \tag{D3}$$

The environmental noise comes from the switching between the $N+1$ gene configurations; each gene switches between its on and off states independently. Following the earlier examples, one expects a contribution $2k_0k_1(b_0-b_1)^2/\lambda(k_0+k_1)^3$ to the variance of the environmental noise from each gene so that the total variance is

$$g_e(p)^2 = \frac{2Nk_1k_0(b_0-b_1)^2}{\lambda(k_0+k_1)^3}. \tag{D4}$$

We note that the relative fluctuations of the total production rate [i.e., the ratio $g_e(p)/Nb_{\rm avg}$] scale as $N^{-1/2}$.

Mathematically, the transition rate matrix for the $N+1$ environmental states may be written as the tridiagonal matrix

$$\begin{aligned}
A_{\sigma\to\sigma-1} &= \lambda k_0\sigma \quad \text{for } \sigma \geqslant 1,\\
A_{\sigma\to\sigma+1} &= \lambda k_1(N-\sigma) \quad \text{for } \sigma \leqslant N-1,\\
A_{\sigma\to\sigma\pm j} &= 0 \quad \text{for } j \geqslant 2,
\end{aligned}\tag{D5}$$

together with the convention $A_{\sigma\to\sigma} = -A_{\sigma\to\sigma-1} - A_{\sigma\to\sigma+1}$. The formalism of Secs. II B and III can then be applied, but becomes algebraically tedious. Using numerical algebra packages, we have verified Eq. (D4) up to $N = 100$.

### 2. Staged switching of the environment

In many situations the switching between environmental states is not purely Markovian. Periodic switching between environmental states has been considered in experimental and theoretical studies of bacterial populations, for example, the presence or absence of antibiotic treatment according to a periodic protocol. As a bet-hedging strategy, the bacteria respond to time-dependent external stresses with phenotypic heterogeneity [9,59,77–79]. In this context it is therefore important to be able to study stochastic populations coupled to environments with non-Markovian dynamics.

In this Appendix we consider an example in which there are two distinct environmental conditions, labeled 0 and 1. In contrast with the previous examples, each of these conditions consists of several identical internal states (or stages), which are traversed in sequence. Similar setups have been used to

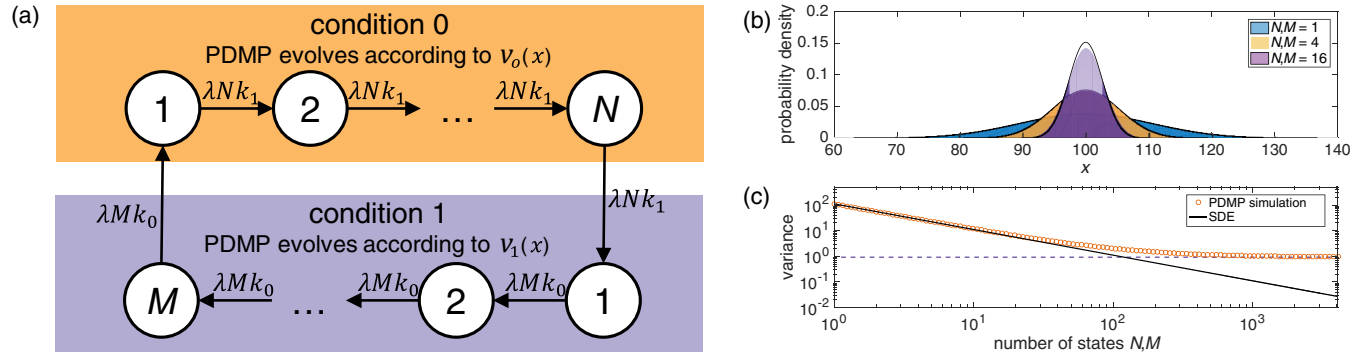


FIG. 6. (a) Schematic illustrating an environment with two distinct conditions, with $N$ and $M$ identical stages, respectively. (b) Stationary distribution for different values of $N = M$. Histograms show the results of simulations and lines are from the theory described in the text. (c) Variance of the stationary distribution as a function of $N$ (again for the case $N = M$). The black line shows the results of the theory and orange circles are from simulations of the piecewise-deterministic Markov process. The parameters $N$ and $M$ have been generalized to include noninteger values, by considering $\gamma$-distributed waiting-time distributions in the two conditions (see the text). The dashed line shows the variance of the limit cycle obtained in the limit of a periodic environment. The parameters are $b_0 = 100/3$, $b_1 = 500/3$, and $\lambda k_0 = \lambda k_1 = 20$.

model dynamics which fall between the purely periodic and purely Markovian limits (see, e.g., Refs. [9,80,81]).

The model is illustrated in Fig. 6(a). There are $N$ environmental states which correspond to environmental condition 0 and $M$ states that correspond to environmental condition 1. States in condition 0 transition to the next state with rate $\lambda k_1 N$ and states corresponding to condition 1 transition to the next state with rate $\lambda k_0 M$. The environment cycles through all states in order, as indicated in the figure.

In this way, the time spent in condition 0 before switching to 1 is $\Gamma(N, \lambda N k_1)$ distributed and similarly the time spent in condition 1 follows a $\Gamma(M, \lambda M k_0)$ distribution. Independent of $N$ and $M$, the environment spends an average time $(\lambda k_1)^{-1}$ in condition 0 before it switches to 1 and then an average time $(\lambda k_0)^{-1}$ in condition 1 before it switches back to condition 0. Increasing the number of states $N$ and $M$ leads to an increased regularity of time spent in each condition. The limit $N, M \to \infty$ in particular corresponds to periodic switching between the two conditions.

For simplicity, we disregard intrinsic noise in this example and focus on a piecewise-deterministic process. We assume that the dynamics is given by $\dot{x} = v_0(x)$ if the environment is in condition 0 and by $\dot{x} = v_1(x)$ if it is in condition 1. We use a symbolic algebra package to solve Eq. (4), where the operator $\mathcal{M}_\sigma$ is replaced by the Liouville operator $\mathcal{L}_\sigma = -\partial_x v_\sigma(x)$. We use this to derive an SDE in the limit of fast but finite environmental dynamics. We find

$$\dot{x} = v_{\rm avg}(x) + g_e(x)\eta(t), \tag{D6}$$

where $\eta(t)$ is white Gaussian noise and the drift and diffusion terms are given by

$$v_{\rm avg}(x) = \frac{k_0 v_0(x) + k_1 v_1(x)}{k_0 + k_1}, \quad g_e(x) = \lambda^{-1/2}\sqrt{\frac{k_1 k_0 (N+M)[v_0(x) - v_1(x)]^2}{NM(k_1 + k_0)^3}}. \tag{D7}$$

We have not attempted to formally prove this for general $N$ and $M$; rather, we tested this result for a range of combinations $N, M < 150$ and found it to be true for all tested values.

In Fig. 6(b) we use a specific example, where the drift is $v_0(x) = b_0 - x$ and $v_1(x) = b_1 - x$. In this figure we compare the stationary distributions obtained from simulation of the PDMP with the stationary distribution obtained analytically from solving the one-dimensional Fokker-Planck equation for Eq. (D6). We show these data for different choices of $N$ and $M$ in Fig. 6(b), restricting the values to $N = M$ for simplicity.

Similarly, we compare the variance of the stationary distributions from the PDMP and the SDE in Fig. 6(c). The parameters $\lambda$, $k_1$, and $k_0$ are kept fixed; we focus again on the case $N = M$ and vary this number of internal states. Analytical results from the SDE and numerical simulation of the PDMP agree well for $N, M < 100$, but there are deviations when $N = M$ becomes large. This is due to fact that the PDMP tends to a deterministic limit cycle; this limit cycles leads to a finite variance of the corresponding distribution, indicated by the dashed line of Fig. 6(c). This limit cycle dynamics is not captured by the SDE.

The model as described above is only defined for integer values of $N$ and $M$. However, the distribution of waiting times in either environmental condition can be generalized to the case of $\gamma$ distributions with noninteger shape parameters. The interpretation as a series of internal states within conditions $\sigma = 0$ and $\sigma = 1$ then no longer holds, but simulations of the model can still be carried out, drawing waiting times directly from the appropriate $\gamma$ distributions. The SDE (D7) remains unaltered and it provides an accurate description of the dynamics of the model also when $N$ and $M$ are not integers. This can be seen in Fig. 6(c), where many of the markers (circles) correspond to simulations for noninteger values of $N$ and $M$.

[1] C. W. Gardiner, *Handbook of Stochastic Methods* (Springer, Berlin, 2004).
[2] N. G. van Kampen, *Stochastic Processes in Physics and Chemistry* (North-Holland, Amsterdam, 2007).
[3] H. Risken, *The Fokker-Planck Equation: Methods of Solution and Applications* (Springer, Berlin, 1989).
[4] E. Kussell, R. Kishony, N. Q. Balaban, and S. Leibler, Genetics **169**, 1807 (2005).
[5] E. Kussell and S. Leibler, Science **309**, 2075 (2005).
[6] S. Leibler and E. Kussell, Proc. Natl. Acad. Sci. USA **107**, 13183 (2010).
[7] P. Thomas, N. Popović, and R. Grima, Proc. Natl. Acad. Sci. USA **111**, 6994 (2014).
[8] T. B. Kepler and T. C. Elston, Biophys. J. **81**, 3116 (2001).
[9] M. Thattai and A. Van Oudenaarden, Genetics **167**, 523 (2004).
[10] P. S. Swain, M. B. Elowitz, and E. D. Siggia, Proc. Natl. Acad. Sci. USA **99**, 12795 (2002).
[11] M. Assaf, E. Roberts, Z. Luthey-Schulten, and N. Goldenfeld, Phys. Rev. Lett. **111**, 058102 (2013).
[12] A. Duncan, S. Liao, T. Vejchodský, R. Erban, and R. Grima, Phys. Rev. E **91**, 042111 (2015).
[13] M. Assaf, M. Mobilia, and E. Roberts, Phys. Rev. Lett. **111**, 238101 (2013).
[14] P. Ashcroft, P. M. Altrock, and T. Galla, J. R. Soc. Interface **11**, 20140663 (2014).
[15] K. Wienand, E. Frey, and M. Mobilia, Phys. Rev. Lett. **119**, 158301 (2017).
[16] R. West, M. Mobilia, and A. M. Rucklidge, Phys. Rev. E **97**, 022406 (2018).
[17] A. J. Black and A. J. McKane, J. Theor. Biol. **267**, 85 (2010).
[18] C. Escudero and J. Á. Rodríguez, Phys. Rev. E **77**, 011130 (2008).
[19] M. Assaf, A. Kamenev, and B. Meerson, Phys. Rev. E **78**, 041123 (2008).
[20] Q. Luo and X. Mao, J. Math. Anal. Appl. **334**, 69 (2007).
[21] C. Zhu and G. Yin, J. Math. Anal. Appl. **357**, 154 (2009).
[22] J. Chiquet and N. Limnios, Stat. Probab. Lett. **78**, 1397 (2008).
[23] J. Chiquet, M. Eid, and N. Limnios, Reliab. Eng. Syst. Safe. **93**, 1801 (2008).
[24] J. Chiquet, N. Limnios, and M. Eid, J. Stat. Plan. Infer. **139**, 1657 (2009).
[25] A. Lorton, M. Fouladirad, and A. Grall, Eur. J. Oper. Res. **225**, 443 (2013).
[26] H. Zhang, F. Dufour, Y. Dutuit, and K. Gonzalez, J. Risk Reliab. **222**, 545 (2008).
[27] A. Lorton, M. Fouladirad, and A. Grall, Proc. Inst. Mech. Eng. O **227**, 434 (2013).
[28] P. C. Bressloff, Phys. Rev. E **94**, 042129 (2016).
[29] M. Assaf, E. Roberts, and Z. Luthey-Schulten, Phys. Rev. Lett. **106**, 248102 (2011).
[30] E. Roberts, S. Be'er, C. Bohrer, R. Sharma, and M. Assaf, Phys. Rev. E **92**, 062717 (2015).
[31] P. C. Bressloff and J. M. Newby, Phys. Rev. E **89**, 042701 (2014).
[32] P. C. Bressloff, Phy. Rev. E **95**, 012124 (2017).
[33] P. C. Bressloff, Phys. Rev. E **95**, 012138 (2017).
[34] J. Bowen, A. Acrivos, and A. Oppenheim, Chem. Eng. Sci. **18**, 177 (1963).
[35] L. A. Segel and M. Slemrod, SIAM Rev. **31**, 446 (1989).
[36] P. G. Hufton, Y. T. Lin, and T. Galla, preceding paper, Phys. Rev. E **99**, 032121 (2019).
[37] M. H. Davis, J. R. Stat. Soc. Ser. B **46**, 353 (1984).
[38] S. Zeiser, U. Franz, O. Wittich, and V. Liebscher, IET Syst. Biol. **2**, 113 (2008).
[39] N. Friedman, L. Cai, and X. S. Xie, Phys. Rev. Lett. **97**, 168302 (2006).
[40] H. Ge, H. Qian, and X. S. Xie, Phys. Rev. Lett. **114**, 078101 (2015).
[41] C. Jia, Phys. Rev. E **96**, 032402 (2017).
[42] C. Jia, M. Q. Zhang, and H. Qian, Phys. Rev. E **96**, 040402 (2017).
[43] U. Herbach, A. Bonnaffoux, T. Espinasse, and O. Gandrillon, BMC Syst. Biol. **11**, 105 (2017).
[44] Y. T. Lin, P. G. Hufton, E. J. Lee, and D. A. Potoyan, PLOS Comput. Biol. **14**, e1006000 (2018).
[45] Y. T. Lin and N. E. Buchler, J. R. Soc. Interface **15**, 20170804 (2018).
[46] X. Mao and C. Yuan, *Stochastic Differential Equations with Markovian Switching* (World Scientific, Singapore, 2006).
[47] D. A. Potoyan and P. G. Wolynes, J. Chem. Phys. **143**, 195101 (2015).
[48] P. G. Hufton, Y. T. Lin, T. Galla, and A. J. McKane, Phys. Rev. E **93**, 052119 (2016).
[49] P. Thomas, A. V. Straube, and R. Grima, BMC Syst. Biol. **6**, 39 (2012).
[50] P. Thomas, R. Grima, and A. V. Straube, Phys. Rev. E **86**, 041110 (2012).
[51] A. Kamenev, B. Meerson, and B. Shklovskii, Phys. Rev. Lett. **101**, 268103 (2008).
[52] J. M. Newby and P. C. Bressloff, Bull. Math. Biol. **72**, 1840 (2010).
[53] E. L. Haseltine and J. B. Rawlings, J. Chem. Phys. **117**, 6959 (2002).
[54] C. V. Rao and A. P. Arkin, J. Chem. Phys. **118**, 4999 (2003).
[55] J. Goutsias, J. Chem. Phys. **122**, 184102 (2005).
[56] H. Qian, P.-Z. Shi, and J. Xing, Phys. Chem. Chem. Phys. **11**, 4861 (2009).
[57] C. D. Pahlajani, P. J. Atzberger, and M. Khammash, J. Theor. Biol. **272**, 96 (2011).
[58] J. Kim, K. Josic, and M. R. Bennett, Biophys. J. **107**, 783 (2014).
[59] P. G. Hufton, Y. T. Lin, and T. Galla, J. Stat. Mech. (2018) 023501.
[60] S. Masui, Y. Nakatake, Y. Toyooka, D. Shimosato, R. Yagi, K. Takahashi, H. Okochi, A. Okuda, R. Matoba, A. A. Sharov, M. S. H. Ko, and H. Niwa, Nat. Cell Biol. **9**, 625 (2007).
[61] T. Kalmar, C. Lim, P. Hayward, S. Muñoz-Descalzo, J. Nichols, J. Garcia-Ojalvo, and A. Martinez Arias, PLOS Biol. **7**, e1000149 (2009).
[62] N. E. Buchler, U. Gerland, and T. Hwa, Proc. Natl. Acad. Sci. USA **100**, 5136 (2003).
[63] L. Cai, N. Friedman, and X. S. Xie, Nature (London) **440**, 358 (2006).
[64] B. Munsky, Z. Fox, and G. Neuert, Methods **85**, 12 (2015).
[65] M. Gómez-Schiavon, L.-F. Chen, A. E. West, and N. E. Buchler, Genome Biol. **18**, 164 (2017).

[66] T. S. Gardner, C. R. Cantor, and J. J. Collins, Nature (London) **403**, 339 (2000).
[67] D. M. Roma, R. A. O'Flanagan, A. E. Ruckenstein, A. M. Sengupta, and R. Mukhopadhyay, Phys. Rev. E **71**, 011902 (2005).
[68] E. Roberts, A. Magis, J. O. Ortiz, W. Baumeister, and Z. Luthey-Schulten, PLOS Comput. Biol. **7**, e1002010 (2011).
[69] J. N. Weiss, FASEB J. **11**, 835 (1997).
[70] S. Karapetyan and N. E. Buchler, Phys. Rev. E **92**, 062712 (2015).
[71] A. Lipshtat, A. Loinger, N. Q. Balaban, and O. Biham, Phys. Rev. Lett. **96**, 188101 (2006).
[72] P. B. Warren and P. R. ten Wolde, J. Phys. Chem. B **109**, 6812 (2005).
[73] J. Chiquet and N. Limnios, Methodol. Comput. Appl. Probab. **8**, 431 (2006).
[74] Y. Lin and J. Yang, AIAA J. **23**, 117 (1985).
[75] B. Spencer, Jr. and J. Tang, J. Eng. Mech. **114**, 2134 (1988).
[76] R. Capocelli and L. Ricciardi, Theor. Popul. Biol. **5**, 28 (1974).
[77] M. Acar, J. T. Mettetal, and A. Van Oudenaarden, Nat. Genet. **40**, 471 (2008).
[78] O. Gefen and N. Q. Balaban, FEMS Microbiol. Rev. **33**, 704 (2009).
[79] P. Patra and S. Klumpp, Phys. Biol. **12**, 046004 (2015).
[80] E. A. Korobkova, T. Emonet, H. Park, and P. Cluzel, Phys. Rev. Lett. **96**, 058105 (2006).
[81] A. J. Black, A. J. McKane, A. Nunes, and A. Parisi, Phys. Rev. E **80**, 021922 (2009).